Journal of Power Sources 224 (2013) 66–71

Contents lists available at SciVerse ScienceDirect

Journal of Power Sources

journal homepage: www.elsevier.com/locate/jpowsour

Short communication

High-performance Pd@PtRu/C catalyst for the anodic oxidation of methanol prepared by decorating Pd/C with a PtRu shell

Yan-Ni Wu [a,*], Shi-Jun Liao [b,**], Hai-Fu Guo [a], Xiang-Ying Hao [a]

[a] School of Chemistry and Chemical Engineering, Zhao Qing University, Guangdong, Zhao Qing 526061, China
[b] School of Chemistry and Chemical Engineering, South China University of Technology, Guangdong, Guangzhou 510640, China

HIGHLIGHTS

- Core–shell Pd@PtRu/C catalyst was prepared by a two-step colloidal method.
- The mass activity for Pd@PtRu/C catalyst is about 1.67 times as large as PtRu/C.
- The catalyst shows excellent poisoning tolerance as PtRu/C catalyst.
- The interaction of alloy shell with Pd core was revealed by XPS results.

GRAPHICAL ABSTRACT

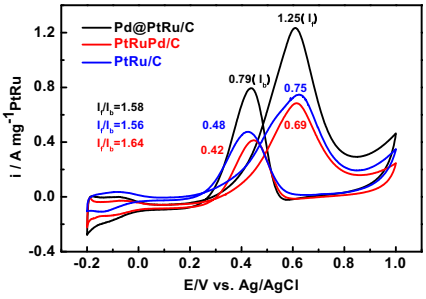

ARTICLE INFO

Article history:
Received 1 August 2012
Received in revised form
17 September 2012
Accepted 18 September 2012
Available online 28 September 2012

Keywords:
Low-platinum catalyst
Methanol oxidation
Core–shell structure
CO tolerance

ABSTRACT

A high-performance, low platinum loading catalyst for the anodic oxidation of methanol, Pd@PtRu/C, is prepared by a two-step colloidal approach. The activity of the Pd@PtRu/C catalyst is 1.67 times and 1.81 times that of PtRu/C and PtRuPd/C catalysts, respectively. The catalysts are characterized by TEM, XPS, and XRD. The active components are dispersed on the surface of the carbon support very well, yielding a particle size of ca. 4.7 nm and a shell thickness of ca. 0.25 nm. The catalyst's high activity may be attributed to the high exposure and dispersion of PtRu, as well as the interaction of PtRu in the shell layer with Pd in the core, resulting from the catalyst's core–shell structure.

1. Introduction

For high activity and good tolerance to carbonaceous species poisoning, PtRu alloy is a well known anode catalyst in direct methanol fuel cells (DMFCs) [1–7]. During the anodic oxidation of methanol in DMFCs catalyzed by a monometal platinum catalyst, the catalyst is easily poisoned by CO or other intermediates generated from the oxidation of methanol. Ru is recognized as the best metal to combine with Pt to minimize this poisoning effect through "the bifunctional mechanism" [1,8]. Many efforts have been focused on the preparation of novel PtRu catalysts and the improvement of PtRu catalysts by adding a third component—for example, depositing very thin PtRu nanoplatelets on carbon nanoparticles [9], or alloying PtRu with Mo [10], TiO_2 [11], or CeO_2 [12]. PtRu-based alloys used as anode catalysts yield improved CO tolerance or enhanced activity for methanol oxidation. However, they are bulky particles, resulting in low utilization efficiency of the noble metals.

* Corresponding author. Tel.: +86 758 2716357.
** Corresponding author. Fax: +86 20 87113586.
E-mail addresses: yanniwu@163.com (Y.-N. Wu), chsjliao@scut.edu.cn (S.-J. Liao).

0378-7753/$ – see front matter © 2012 Elsevier B.V. All rights reserved.
http://dx.doi.org/10.1016/j.jpowsour.2012.09.079

To develop a novel catalyst with high activity, low noble metal usage, and high poisoning tolerance, an alternative strategy has been adopted: preparation of a core–shell structure catalyst with a PtRu alloy shell. Core–shell nanosized particles that have large surface-to-volume ratios and special binding sites for fine particles in homogeneous and heterogeneous catalysis, and that have the active metal (e.g., Pt) distributed only on their surface, provide the opportunity to increase Pt utilization and thus lower the noble metal loading [13,14]. The core–shell structure may also provide aggregation resistance [15]. Core–shell structured catalysts, such as Pd/Pt core–shell nanowire arrays [6], Au@Pt/C [16,17], Ni@Pt [18], Ni@Pd [19], Pt@Ru/C [20], Pd_4Co [21], and so forth, have been widely investigated for methanol oxidation, but most with a monometal shell showed no obvious improvement in CO tolerance. It is therefore important to develop a type of core–shell catalyst with a PtRu alloy shell. In fact, there have already been a few reports of core–shell catalysts with alloy shells—e.g., PdCu@PtRu [22], Co@Pt–Ru [23], and Pt–Ru@PThB [24]—confirming that a core–shell catalyst with an alloy shell not only achieves the high performance and high utilization of a noble metal, but also improves tolerance to poisonous species.

To decrease cost while improving catalytic activity, Pd is expected to be a good fit with Pt, as the two metals have a lattice mismatch of only 0.77%; thus, the Pd surface favors the reduction of Pt [18,25]. More significantly, Pd nanocrystals are much cheaper than Pt nanocrystals and have good electrochemical stability, making Pd the ideal core element for the synthesis of a PtRu alloy-shelled core–shell catalyst.

Based on the foregoing, we fabricated a PtRu alloy-shelled core–shell structure catalyst by decorating Pd core nanoparticles with a PtRu shell via a two-step colloidal method. This method of preparing Pd@PtRu/C leads to PtRu islands occurring selectively on the pre-formed Pd surface, favoring synergetic catalytic effects between the Pd core and PtRu shell. The Pd@PtRu/C catalyst synthesized in this work showed both remarkable catalytic activity and good tolerance to CO poisoning during methanol oxidation.

2. Experimental

2.1. Preparation of Pd@PtRu/C electrocatalyst

Carbon-supported Pd/C, which was used as the core, was prepared by an organic colloid method [26,27]. Palladium chloride ($PdCl_2$) and sodium citrate were dissolved in ethylene glycol (EG), then stirred for 30 min. Afterward, Vulcan® XC72 carbon black (Cabot Corp., BET: 237 $m^2\ g^{-1}$, denoted as C) was added to the mixture under stirring (Pd loading of 12%). The pH of the mixed solution was adjusted to >10 by the drop-wise addition of a 5 wt% KOH/EG solution under stirring. The solution was then placed into a Teflon®-lined autoclave and reacted at 160 °C for 8 h, followed by filtering, washing and vacuum drying at 70 °C, yielding the Pd/C. The Pd@PtRu/C catalyst was prepared by depositing a shell layer of PtRu alloy on the surface of the Pd/C (Pd, Pt, and Ru metal loadings of 12%, 5%, and 3%, respectively, Pt:Ru atomic ratio of 1:1); the procedures were same to those in step 1 for the preparation of Pd/C, but using Pd/C instead of carbon, and using Pt and Ru precursors instead of Pd precursors.

The total metal loading was ca. 20 wt% and the nominal Pt content was ca. 5 wt%. For comparison, 20 wt% PtRu/C (Pt:Ru atomic ratio of 1:1) and PtRuPd/C (same metal loading as for Pd@PtRu/C) were prepared using the same approach.

2.2. Measurements

Information on the particle size and shape of the prepared catalysts was obtained using scanning transmission electron microscopy (Hitachi HD-2000 STEM) at 200 kV, and transmission electron microscopy (JEOL JEM-2010HR, Japan).

The phase structure was identified by X-ray diffraction (XRD) measurement using a Shimadzu XD-3A X-ray diffractometer (Japan) with a filtered Cu-Kα radiation source, operated at 35 kV and 30 mA. Diffraction patterns were collected from 20° to 80° at a scanning rate of 4° min^{-1} and with a step size of 0.01°.

An IM6e electrochemical workstation (Zahner, Germany) and a standard three-electrode electrochemical cell were used to evaluate the catalysts' electrochemical reactivity by cyclic voltammetry (CV) at room temperature. A platinum wire and an Ag/AgCl electrode were used as the counter and reference electrodes, respectively. The working electrode was a glassy carbon disk covered with a thin layer of Nafion®-impregnated catalyst. The thin-film electrode was prepared as follows: 5 mg of catalyst was dispersed in 1 mL Nafion®/ethanol (0.25% Nafion®) by sonication for 30 min, and 6 μL of the dispersion ink was applied onto a glassy carbon working electrode (diameter of 5 mm) using a pipette. A CV test was conducted at 50 mV s^{-1} in a solution of 0.5 M H_2SO_4 or 0.5 M H_2SO_4 + 0.5 M CH_3OH, in the potential range of −0.2 to 1.0 V. High-purity N_2 was used before and during the measurement to purge the electrolyte. The PtRu loadings of the PtRu/C and Pd@PtRu/C catalysts on the electrode surface were 0.006 and 0.0024 mg PtRu cm^{-2}, respectively, and same PtRu loadings for the PtRuPd/C catalyst.

3. Results and discussion

Fig. 1 presents the XRD patterns of the prepared Pd@PtRu/C, Pd/C, PtRu/C, and PtRuPd/C. The peak at 25.3° can be attributed to the (002) diffraction of the carbon supports. The other diffraction peaks at Bragg angles of 24.5°, 39.8°, 46.3°, and 67.6° are assigned to the (111), (200), and (220) facets of Pd with a face-centered cubic lattice structure, revealing that the Pd@PtRu/C catalyst still has the structure of palladium, although a thin PtRu alloy layer decorates the surface of the palladium nanoparticles. The broadened peak of PtRu/C around 30°–50° is due to the presence of small particles in the PtRu/C. The average particle sizes of the Pd/C, PtRu/C, PtRuPd/C, and Pd@PtRu/C, estimated from the XRD data using Jade software, are 4.2, 2.7, 5.8, and 4.7 nm, respectively; the size increase from Pd/C to Pd@PtRu/C confirms that PtRu alloy decorated the surface of the Pd nanoparticles in the second preparation step. The

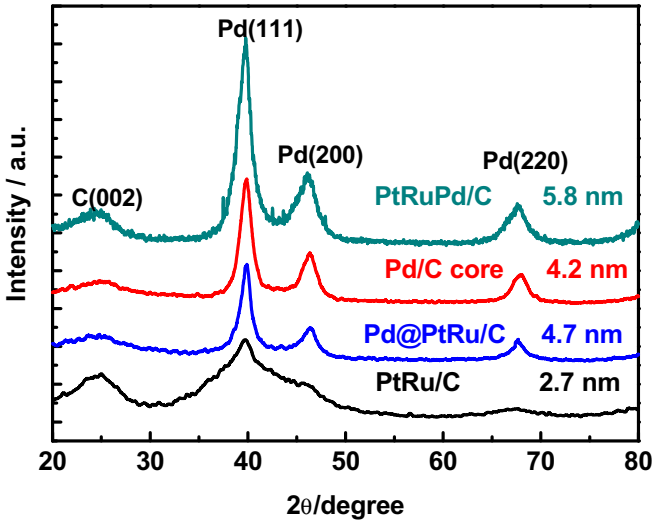

Fig. 1. XRD patterns of Pd/C, PtRu/C, PtRuPd/C and Pd@PtRu/C catalysts.

thickness of the PtRu shell layer was ca. 0.25 nm. It is notable that the particle size of Pd@PtRu/C (4.7 nm) is much smaller than that of PtRuPd/C (5.8 nm) due to the special core–shell structure. Furthermore, we found that the diffraction peak (220) for both Pd@PtRu/C and PtRuPd/C had a slightly negative shift compared to that of Pd/C.

Fig. 2 shows TEM images of the Pd@PtRu/C (A, B), PtRu/C (C, D), and PtRuPd/C (E, F) catalysts. It can be seen in Fig. 2A and B that active components are well dispersed on the carbon support and have a very narrow particle size distribution. It is clear that the active components dispersion of Pd@PtRu/C catalyst is much better than that of PtRuPd/C, but less desirable than that of PtRu/C. The average particle sizes of active components for catalysts PtRuPd/C, Pd@PtRu/C, and PtRu/C are ca. 5.6, 4.5, and 2.5 nm, respectively; these values are in good agreement with the XRD results. The PtRu-rich shell on the Pd/C core could not be observed due to the particle's very small size and very thin shell layer, and to the similar lattice parameters of Pt and Pd. However, the X-ray photoelectron spectroscopy (XPS) results revealed the existence of Pt and Ru; thus, it is reasonable to suggest that the PtRu would be reduced and then cover the core Pd particles, because it is suggested that depositing the shell metals on the metal core will be easier than on the carbon support [27].

To obtain information about the surface composition, the surface electronic structure of the PtRuPd/C and Pd@PtRu/C

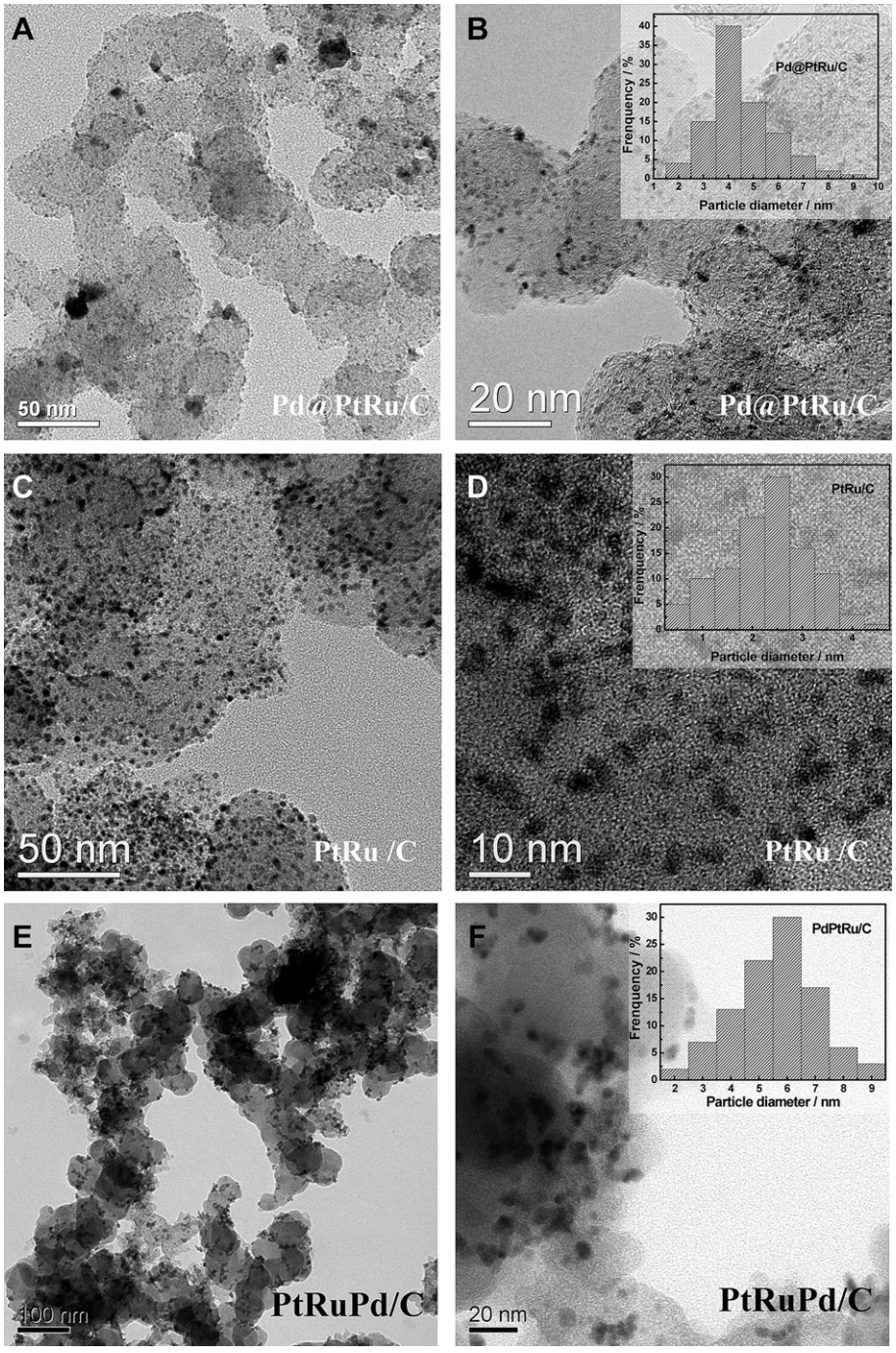

Fig. 2. TEM images of the Pd@PtRu/C (A, B), PtRu/C (C, D) and PtRuPd/C (E, F) catalysts and the corresponding particle size distribution.

catalysts was further evaluated by XPS. Fig. 3A and B shows the wide-scan XPS spectra of PtRuPd/C and Pd@PtRu/C. The detected atomic ratios of the Pt (0.61) and Ru (0.13) peaks in Pd@PtRu/C are obviously stronger than those of the Pt (0.35) and Ru (0.07) peaks in PtRuPd/C, while the detected atomic ratio of Pd (0.70) in Pd@PtRu/C is much weaker than that of Pd (2.0) in PtRuPd/C, demonstrating that the surface of Pd@PtRu/C is enriched by PtRu. Since the recipe atomic ratio of Pt:Pd:Ru in both PtRuPd/C and Pd@PtRu/C catalysts is the same, the surface-enriched PtRu and the surface-poor Pd are possible indications of PtRu covering the preformed Pd nanoparticles. Thus, the results support the suggestion that the Pd@PtRu/C catalyst has a clearly identifiable core–shell structure.

The Ru 3d spectra overlap with the C 1s spectra, making it difficult to quantify the binding energy states of Ru. Fig. 3C shows the Ru 3d spectra. Hence, the Ru in the PtRuPd/C and Pd@PtRu/C catalysts can still be clearly identified.

Fig. 3D–G shows the detailed XPS spectra of Pt 4f and Pd 3d in Pd@PtRu/C and PtRuPd/C; each spectrum was analyzed by deconvolution. For PtRuPd/C (Fig. 3D) after deconvolution, the peaks with binding energies of 71.1 and 74.6 eV are ascribed to metallic Pt, whereas the peaks corresponding to 71.8 and 75.5 eV can be assigned to Pt (II) species in the form of $Pt(OH)_2$ or PtO [28]. But for Pd@PtRu/C, the binding energies of Pt 4f in the shell layer are higher than those of PtRuPd/C, indicating an interaction between Pd and PtRu. Indeed, the positive shift of Pt 4f in the shell layer has been mentioned by other groups [29].

Regarding the binding energy of Pd 3d, we found that the binding energies of Pd in the core of the Pd@PtRu/C catalyst (Fig. 3G) were lower than those of Pd in the PtRuPd/C catalyst (Fig. 3E), which is the reverse of Pt. The negative shift of Pd 3d in the core may result from the interaction between Pd and the Pt and Ru in the alloy.

The XPS results, the catalyst synthesis method, and our previous work all indicate a core–shell structure [30,31]. CV was used to confirm the PtRu-on-Pd/C structure.

The fine structures of the core and shell layers were further characterized using CV, a surface-sensitive technique that detects the electrochemical properties of surface atoms only, rather than of bulk atoms [32]. For comparison, the electrochemical performances of PtRu/C and PtRuPd/C were also investigated. Fig. 4 plots the CV results of the PtRu/C, PtRuPd/C, and Pd@PtRu/C catalysts in N_2-purged 0.5 M H_2SO_4; a large hydrogen oxidation peak for Pd at around −0.2 V can be clearly observed for PtRuPd/C, but for the Pd@PtRu/C sample this peak has disappeared, indicating that the carbon-supported Pd nanoparticles may be covered by a PtRu layer. Furthermore, the CV results demonstrate the multi-metal characteristics of Pd@PtRu/C because it has almost the same CV plot as PtRu/C. The electrochemical surface areas ESA of the catalysts can be calculated by integrating the hydrogen adsorption/desorption charges [33], based on Fig. 4. The S_{ESA} of Pd@PtRu/C (143.3 $m^2\ g^{-1}$ PtRu metal) is much higher than that of PtRu/C (95.1 $m^2\ g^{-1}$ PtRu metal) and PtRuPd/C (83.7 $m^2\ g^{-1}$ PtRu metal). During the preparation of Pd@PtRu/C, Pd/C is prepared first and the active sites of the carbon support are mainly occupied by Pd nanoparticles. Consequently, the addition of H_2PtCl_6 and $RuCl_3$ causes the Pt and Ru ions to be reduced largely on the pre-formed Pd surfaces, leaving only occasional isolated PtRu nanoparticles. Hence, the cyclic voltammogram of Pd@PtRu/C possesses characteristics of both PtRu/C and Pd/C. This result reveals that the PtRu on Pd/C core–shell structure plays a major role in enhancing the ESA because the platinum and ruthenium were highly dispersed on the core Pd surface, and PtRu and Pd had a synergistic effect at the interface. Thus, the core–shell structure, or the pseudo core–shell structure achieved by platinum

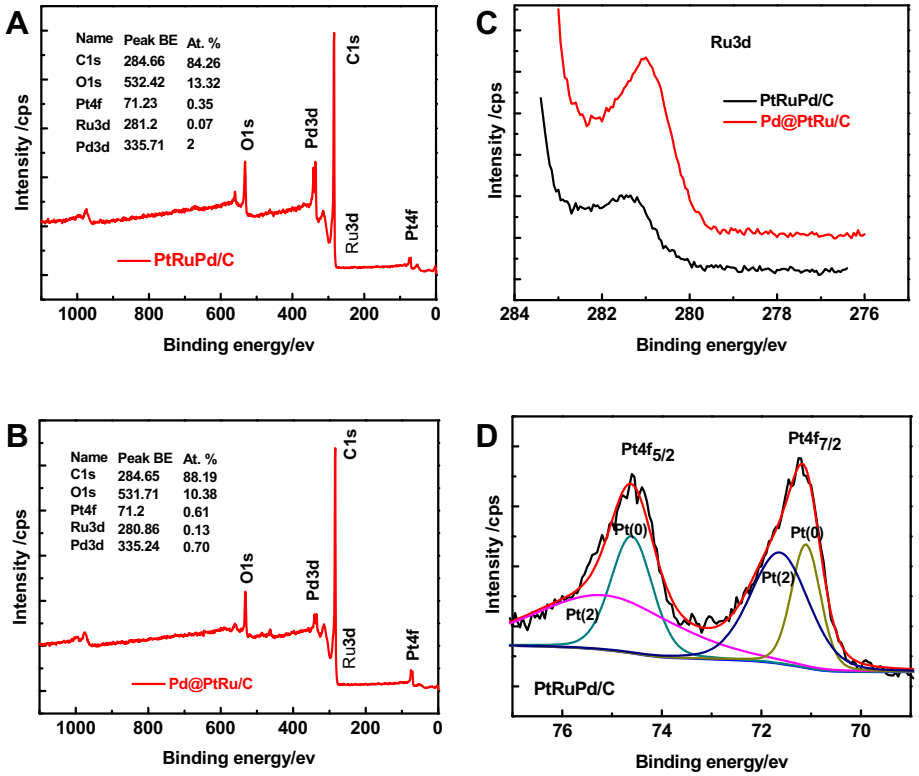

Fig. 3. Survey XPS spectra of the PtRuPd/C (A) and Pd@PtRu/C (B) catalysts, the Ru 3d core level XPS spectra of the catalysts PtRuPd/C and Pd@PtRu/C (C); the Pt 4f core level XPS spectra of PtRuPd/C (D) and Pd@PtRu/C (E); the Pd 3d core level XPS spectra of the PtRuPd/C (F) and Pd@PtRu/C (G) catalysts.

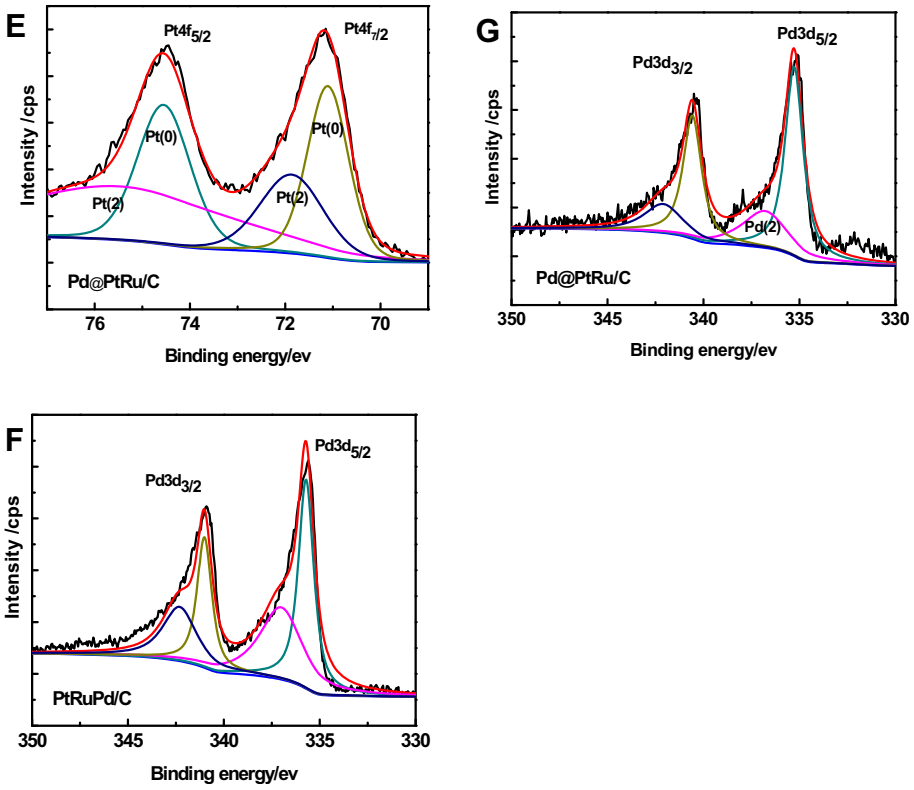

Fig. 3. (*continued*).

and ruthenium covering the surface of the Pd/C cores in Pd@PtRu/C, was indirectly confirmed by CV in 0.5 M H_2SO_4 solution.

The effect of the core–shell structure on the electrocatalytic activity of Pd@PtRu/C was investigated in a 0.5 M H_2SO_4 + 0.5 M CH_3OH solution. As shown in Fig. 5, the core–shell structured Pd@PtRu/C catalyst exhibited very high activity toward the anodic oxidation of methanol.

The typical cyclic voltammograms of Pd@PtRu/C, PtRuPd/C, and PtRu/C for methanol electrooxidation in 0.5 M H_2SO_4 + 0.5 M CH_3OH solution are presented in Fig. 5. For the core–shell structured Pd@PtRu/C catalyst, the forward-sweeping peak current density reaches 1.25 A mg^{-1} PtRu, which is about 1.67 times and 1.81 times as large as that of PtRu/C (0.75 A mg^{-1} PtRu) and PtRuPd/C (0.69 mA mg^{-1} PtRu), respectively. The core–shell structured Pd@PtRu/C catalyst clearly shows superior activity to the PtRu/C and PtRuPd/C catalysts for the anodic oxidation of methanol. As mentioned previously, the ESA of Pd@PtRu/C is 1.5 and 1.6 times larger than that of PtRu/C and PtRuPd/C, so the activity results of PtRuPd/C and Pd@PtRu/C seem quite consistent with the ESA results. In addition, the onset potential of methanol oxidation on Pd@PtRu/C (0.19 V) shows a negative shift compared to that of PtRuPd/C (0.21 V), due to the former's core–shell structure. It is generally acknowledged that the peak current for the forward scan (I_f) is due to methanol oxidation and the peak current for the reverse scan (I_b) is associated with the removal of the poisonous CO intermediate [18]. The I_f/I_b ratio is often used to describe tolerance to carbonaceous species poisoning [34]. The I_f/I_b ratio of Pd@PtRu/C is 1.58, which is similar to that of PtRuPd/C (1.56) and slightly lower than that of PtRu/C (1.64), showing that the core–shell structured Pd@PtRu/C catalyst has high activity toward the anodic oxidation of methanol and good tolerance to poisonous species on the catalyst surface.

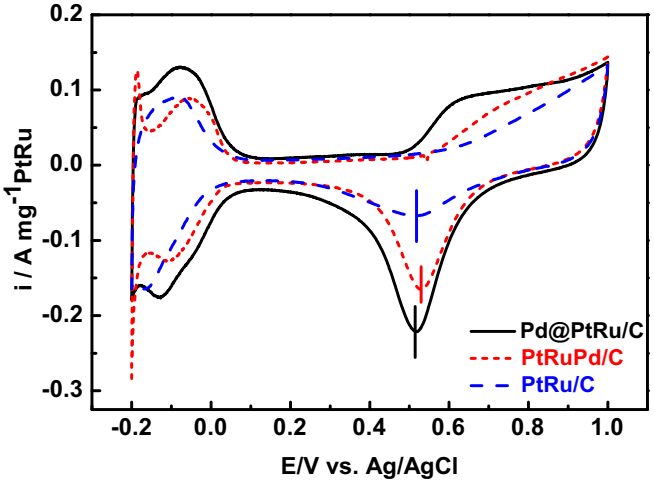

Fig. 4. Cyclic voltammograms of PtRu/C, PtRuPd/C and Pd@PtRu/C in 0.5 M H_2SO_4 under N_2 atmosphere at room temperature; sweep rate = 50 mV s^{-1}.

It should be pointed out that the mass activity of our core shell catalyst Pd@PtRu/C in terms of platinum is higher than that reported previously by other researcher (2.0 A mg^{-1} Pt *vs.* 0.8 A mg Pt^{-1}) [22].

Because Pd is inactive for methanol oxidation [35], the activity of PtRuPd/C is a little lower than that of PtRu/C. As previously mentioned, the activity of Pd@PtRu/C showed 1.81 times higher than PtRuPd/C, indicating that the activity of Pd@PtRu/C was greatly enhanced by the core–shell structure. One reason is that the core–shell structure increases the surface-to-volume ratio; another reason is that the Pd core can have a synergistic electronic effect with the PtRu in the shell layer, making the electrocatalyst more

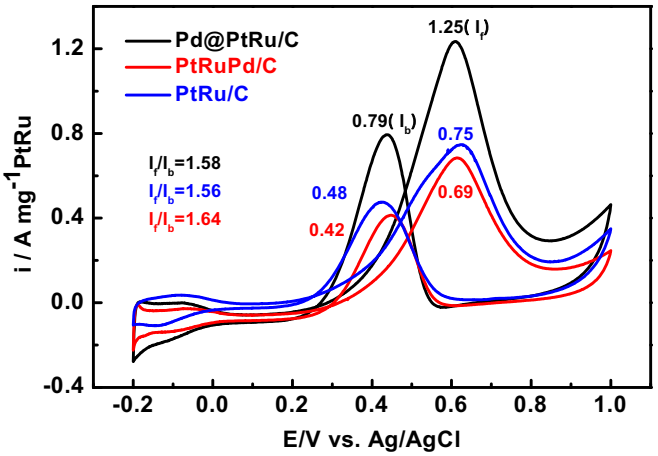

Fig. 5. Cyclic voltammograms of Pd@PtRu/C, PtRuPd/C and PtRu/C in 0.5 M H_2SO_4 + 0.5 M CH_3OH at room temperature; sweep rate = 50 mV s^{-1}.

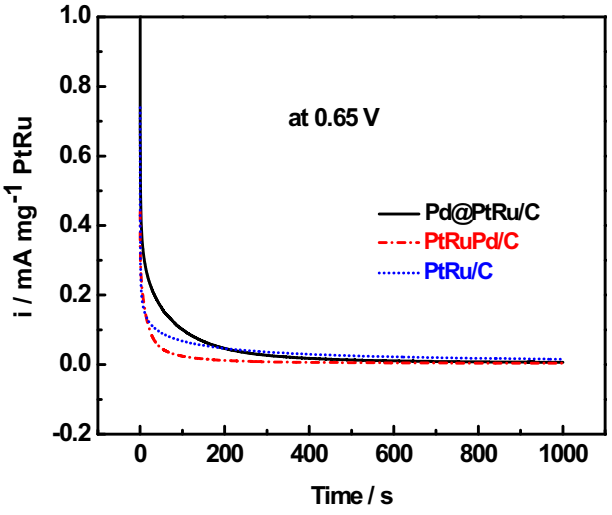

Fig. 6. The chronoamperometric curves for the anodic oxidation of methanol on PtRu/C, PtRuPd/C and Pd@PtRu/C electrodes of 0.5 M CH_3OH in 0.5 M H_2SO_4 solution for 1000 s; fixed potential = 0.65 V, rotation speed = 300 rpm.

efficient. The remarkably high mass-specific oxidation current for the methanol oxidation reaction and the good tolerance to CO_{ads} may be attributable to both the high dispersion of platinum and ruthenium on the Pd core and the strong interaction between the outer PtRu shell and the inner Pd core.

Fig. 6 shows the chronoamperometric curves of methanol anodic oxidation on PtRu/C, PtRuPd/C, and Pd@PtRu/C electrodes at 0.65 V in 0.5 M CH_3OH + 0.5 M H_2SO_4 solution. It is obvious that the Pd@PtRu/C composite electrode shows more stability than the PtRuPd/C electrode under the same experimental conditions. This result further confirms the high activity and stability of the core–shell structured Pd@PtRu/C catalyst.

4. Conclusions

A core–shell structured Pd@PtRu/C catalyst with a PtRu alloy shell was prepared by a two-step colloidal approach. The core–shell structure resulted in a high dispersion of the active components. The catalyst showed significantly enhanced activity for the anodic oxidation of methanol, as well as higher tolerance to poisoning by intermediates generated in the process of anodic methanol oxidation. For the anodic oxidation of methanol, the mass activity of Pd@PtRu/C was 1.67 times as large as that of PtRu/C, and the I_f/I_b ratio was as high as 1.58. Furthermore, various characterization results revealed the core–shell structure and the interaction between shell and core. Its high activity, combined with good poisoning tolerance and good stability, makes Pd@PtRu/C a promising and competitive low-Pt catalyst for PEMFC or DMFC applications.

Acknowledgments

We would like to thank the National Scientific Foundation of China (NSFC Project Nos. 20673040, 20876062), the Guangdong Provincial Scientific Foundation (Project No. 36055), and the Guangdong Provincial Fuel Cells Critical Laboratory Foundation for financial support of this work.

References

[1] R. Chetty, W. Xia, S. Kundu, M. Bron, T. Reinecke, W. Schuhmann, M. Muhler, Langmuir 25 (2009) 3853–3860.
[2] S. Alayoglu, P. Zavalij, B. Eichhorn, Q. Wang, A.I. Frenkel, P. Chupas, ACS Nano 3 (2009) 3127–3137.
[3] S.L. Gojkovic, T.R. Vidakovic, D.R. Durovic, Electrochim. Acta 48 (2003) 3607–3614.
[4] J.W. Guo, T.S. Zhao, J. Prabhuram, R. Chen, C.W. Wong, Electrochim. Acta 51 (2005) 754–763.
[5] T. Iwasita, H. Hoster, A. John-Anacker, W.F. Lin, W. Vielstich, Langmuir 16 (1999) 522–529.
[6] H. Wang, C. Xu, F. Cheng, M. Zhang, S. Wang, S.P. Jiang, Electrochem. Commun. 10 (2008) 1575–1578.
[7] X. Wang, J. Liao, C. Liu, W. Xing, T. Lu, Electrochem. Commun. 11 (2009) 198–201.
[8] M. Wakisaka, S. Mitsui, Y. Hirose, K. Kawashima, H. Uchida, M. Watanabe, J. Phys. Chem. B 110 (2006) 23489–23496.
[9] Y. Ando, K. Sasaki, R. Adzic, Electrochem. Commun. 11 (2009) 1135–1138.
[10] A. Bauer, E.L. Gyenge, C.W. Oloman, J. Power Sources 167 (2007) 281–287.
[11] J.M. Chen, L.S. Sarma, C.H. Chen, M.Y. Cheng, S.C. Shih, G.R. Wang, D.G. Liu, J.F. Lee, M.T. Tang, B.J. Hwang, J. Power Sources 159 (2006) 29–33.
[12] J. Wang, X. Deng, J. Xi, L. Chen, W. Zhu, X. Qiu, J. Power Sources 170 (2007) 297–302.
[13] C. Zhong, M. Maye, Adv. Mater. 13 (2001) 1507–1511.
[14] G.E. Ramirez-Caballero, P.B. Balbuena, Chem. Phys. Lett. 456 (2008) 64–67.
[15] K.C. Pingali, S. Deng, D.A. Rockstraw, Powder Technol. 187 (2008) 19–26.
[16] J. Zeng, J. Yang, J.Y. Lee, W. Zhou, J. Phys. Chem. B 110 (2006) 24606–24611.
[17] N. Kristian, X. Wang, Electrochem. Commun. 10 (2008) 12–15.
[18] X.Z. Fu, Y. Liang, S.P. Chen, J.D. Lin, D.W. Liao, Catal. Commun. 10 (2009) 1893–1897.
[19] Y. Zhao, X. Yang, J. Tian, F. Wang, L. Zhan, Int. J. Hydrogen Energy 35 (2010) 3249–3257.
[20] Y. Li, L. Zheng, S. Liao, J. Zeng, J. Power Sources 196 (2011) 10570–10575.
[21] J.H. Jang, C. Pak, Y.U. Kwon, J. Power Sources 201 (2012) 179–183.
[22] R. Wang, H. Li, H. Feng, H. Wang, Z. Lei, J. Power Sources 195 (2010) 1099–1102.
[23] H. Zhao, L. Li, J. Yang, Y. Zhang, Electrochem. Commun. 10 (2008) 1527–1529.
[24] J.H. Ryu, S.H. Jung, K.S. Sim, S.H. Choi, Appl. Radiat. Isot. 67, 1449–1453.
[25] B. Lim, J. Wang, P.H.C. Camargo, M. Jiang, M.J. Kim, Y. Xia, Nano Lett. 8 (2008) 2535–2540.
[26] S. Liao, K.A. Holmes, H. Tsaprailis, V.I. Birss, J. Am. Chem. Soc. 128 (2006) 3504–3505.
[27] J. Zhang, Y. Mo, M. Vukmirovic, R. Klie, K. Sasaki, R. Adzic, J. Phys. Chem. B 108 (2004) 10955–10964.
[28] C.J. Corcoran, H. Tavassol, M.A. Rigsby, P.S. Bagus, A. Wieckowski, J. Power Sources 195 (2010) 7856–7879.
[29] H. Gao, S. Liao, J. Zeng, Y. Xie, D. Dang, Electrochim. Acta 56 (2011) 2024–2030.
[30] Y.N. Wu, S.J. Liao, Z.X. Liang, L.J. Yang, R.F. Wang, J. Power Sources 194 (2009) 805–810.
[31] Y.N. Wu, S.J. Liao, Y.L. Su, J.H. Zeng, D. Dang, J. Power Sources 195 (2010) 6459–6462.
[32] J. Luo, L. Wang, D. Mott, P.N. Njoki, Y. Lin, T. He, Z. Xu, B.N. Wanjana, I.-I.S. Lim, C.-J. Zhong, Adv. Mater. 20 (2008) 4342–4347.
[33] B. Seger, A. Kongkanand, K. Vinodgopal, P.V. Kamat, J. Electroanal. Chem. 621 (2008) 198–204.
[34] L. Yang, Y. Xiao, G. Zeng, S. Luo, S. Kuang, Q. Cai, Energy Fuels 23 (2009) 3134–3138.
[35] K. Lee, O. Savadogo, A. Ishihara, S. Mitsushima, N. Kamiya, K. Ota, J. Electrochem. Soc. 153 (2006) A20.